Intermolecular Ab Initio Potential and Spectroscopy of the Ground State of HeI_2 Complex Revisited

Leonor García-Gutierrez,[§] Laura Delgado-Tellez,[†] Álvaro Valdés,[‡] Rita Prosmiti,* Pablo Villarreal, and Gerardo Delgado-Barrio

Instituto de Física Fundamental, C.S.I.C., Serrano 123, 28006 Madrid, Spain

Received: February 11, 2009; Revised Manuscript Received: March 24, 2009

The structure, energetics, and spectroscopy of ground-state HeI_2 molecule are analyzed from first principles. Ab initio methodology at CCSD(T) level of theory was employed, and large basis sets were used to compute the interaction energies. Scalar relativistic effects were accounted for by relativistic effective core potentials for the iodine atoms. Recent experimental investigations of the HeI_2 rovibronic spectra have estimated the ground-state binding energies of 16.6 ± 0.6 and 16.3 ± 0.6 cm^{-1} for the T-shaped and linear isomers, respectively. Given the extremely small difference between the two conformers, special attention was paid in the choice of basis sets used and the extrapolation schemes employed, as well as the fitting process for its analytical representation. The complete analytical form is provided, and variational fully quantum mechanical calculations were carried out by using the new parametrized surface, to evaluate vibrationally averaged structures and binding energies for the different conformers. The results obtained are in good accord with recent data available from experimental investigations of the He—I_2 rovibronic spectra.

I. Introduction

Rare-gas—dihalogen van der Waals (vdW) complexes have become prototypes for studying the nature of long-range intermolecular interactions and energy transfer mechanisms. In spite of their simplicity, considerable attention has been paid, both by theory and experiment, to the structure and dynamics of such triatomic systems, and new aspects have recently emerged from such studies. For example, high level ab initio electronic structure calculations have predicted minima for both linear and T-shaped configurations, and theoretical simulation of the B ← X excitation spectrum have confirmed and assigned transitions of such multiple conformers in He—dihalogen molecule complexes.[1−4] Recent experimental studies using laser-induced fluorescence (LIF), action, and two-laser, pump—probe spectroscopy techniques have stabilize ground-state complexes with both linear and T-shaped geometries.[2−6] For most of such systems, for example, $HeBr_2$ and HeICl, the linear isomer has been found to be more strongly bound than the T-shaped one. The only exception was the HeI_2 ground-state complex, for which the binding energy of the T-shaped conformer has been recently measured to be slightly larger than that of the linear one.[6] In particular, Loomis and co-workers[6] estimated a binding energy of 16.3 ± 0.6 cm^{-1} for the linear isomer and 16.6 ± 0.6 cm^{-1} for the T-shaped configuration. In earlier experiments, Levy and co-workers[7] have reported a bond energy of 18.8 ± 0.6 cm^{-1} for the T-shaped structure, and later on, Janda and co-workers[8] have revised it to 17.6 ± 1.0 cm^{-1} by reevaluating the available data.[9] These values are slightly higher, by 1−2 cm^{-1}, than the recent experimental value by Loomis's group.[6]

On the other hand, theoretical data based on ab initio calculations have also been published.[10−12] The latest study[12] predicts two minima for the HeI_2 (X) surface, corresponding to the linear and T-shaped configurations at very similar energies: −43.52 and −37.32 cm^{-1}, respectively, with a relatively low isomerization barrier of 25.64 cm^{-1} above the global linear minimum. Further, bound-state calculations based on this CCSD(T) potential surface reported[12] the existence of both linear and T-shaped isomers, with binding energies of 15.4 and 14.7 cm^{-1}, respectively, with the linear isomer being the most stable. The rather small energy difference (0.7 cm^{-1}) supports the coexistence of the two isomers even at low temperatures. The above estimations do not overlap with the very recent experimental results by Loomis's group.[6] One of the goals of our theoretical studies is to assist the experimental search and assignment of the signatures of different isomers. Thus, further investigation is needed for a more accurate description of the potential energy surface for the ground electronic state of the HeI_2 in order to determine the stability of the two isomers and understand the nature of the underlying intermolecular forces.

In this article, we present new high-level ab initio calculations in order to provide an accurate, global, and reliable surface for the ground state of HeI_2 complex, regarding its dynamics and spectra, with special emphasis on the stability of the two isomers. Up to now, ab initio electronic structure calculations have advanced to a point that they are useful for determining potential surface of rare-gas—dihalogen complexes.[13−21] However, the case of the ground-state HeI_2 presents a challenge for the general theory of intermolecular interactions. The ordering and the extremely small relative stability, predicted by the experiment, of the two isomers will be an additional criterion for evaluating the surface. In this way, we will demonstrate to what extent ab initio computations could be reach. By analyzing the topology of the PES, we were able to rationalize trends and relate them to properties of He—dihalogen molecule clusters family. In our calculations, relativistic effects are included with the use of effective core potentials (ECPs) for I atoms and

* To whom correspondence should be addressed. E-mail: rita@imaff.cfmac.csic.es.
[†] Present address: Hospital del Henares, 28820 Coslada, Madrid, Spain.
[‡] Present address: LIC Gorlaeus Laboratoria, Universiteit Leiden, 2300 RA Leiden, The Netherlands.
[§] Present address: Yukawa Institute For Theoretical Physics, Kyoto University, Kyoto, 606-8502 Japan.

10.1021/jp901250u CCC: $40.75
Published on Web 04/20/2009

TABLE 1: CCSD(T) Interaction Energies for the He—I_2 Molecule Obtained with Different Basis Sets for $r = 2.666$ Å, $\theta = 0$ and 90°, at the Indicated R Distances[a]

ECP	basis		$\theta = 0°$		$\theta = 90°$	
I	I	He	$R = 5$ Å	$R = 5.25$ Å	$R = 3.75$ Å	$R = 4.25$ Å
ECP28MDF	AVTZ-PP[27]	AVTZ	−34.90	−30.28	−25.99	−25.63
ECP28MDF	AVQZ-PP	AVQZ	−38.97	−32.52	−32.84	−28.06
ECP28MDF	AV5Z-PP	AV5Z	−40.79	−33.54	−35.65	−29.10
			−41.29[b]	−33.93[b]	−35.84[b]	−29.26[b]
ECP28MDF	AV5Z-PP	AV5Z+bf	−42.24	−34.50	−35.89	−29.19
ECP28MDF	CBS[345][c,d]	CBS[345]	−41.85	−34.14	−37.29	−29.71
ECP28MDF	CBS[45][e,f]	CBS[45]	−42.64	−34.64	−38.61	−30.20
ECP28MDF	CBS[45][g,f]	CBS[45]	−43.46	−34.80	−37.97	−29.94
ECP46MDF	Dolg[24]	AVQZ	−42.81	−34.70	−36.83	−29.64
ECP46MDF	Dolg	AV5Z	−43.55	−35.10	−37.89	−30.00
ECP46MDF	Dolg	AV5Z+bf	−46.08	−36.71	−38.52	−30.18
ECP46MWB	SDB-AVTZ[26]	AVTZ	−35.58[h]	−30.53[h]	−26.34[h]	−25.74[h]
ECP46MWB	SDB-AVTZ	AV5Z	−38.41[h]	−32.11[h]	−30.73[h]	−27.24[h]
ECP46MWB	SDB-AVTZ	AV5Z+bf	−42.10[h]	−34.44[h]	−36.67[h]	−29.85[h]
ECP46MWB	SDB-AVQZ	AVQZ	−42.72	−34.73	−36.76	−29.69
ECP46MWB	SDB-AVQZ	AV5Z	−43.49	−35.13	−37.85	−30.06
ECP46MWB	SDB-AVQZ	AV5Z+bf	−46.06	−36.76	−38.52	−30.24

[a] bf stands for a (3s3p2d2f1g) set of bond functions. [b] MP4(SDTQ) interaction energies. [c] Reference 31. [d] Extrapolated from AVTZ, AVQZ, and AV5Z values, see text. [e] Reference 32. [f] Extrapolated from AVQZ and AV5Z values, see text. [g] Reference 33. [h] Results from ref 12. CPP correction is not included.

various consistent correlated basis sets for the He atom. Further, different extrapolation schemes are tested in order to check the convergence of the interaction energies in complete basis set (CBS) limit. In the present calculation, we improve our previous one in several respects. We use more accurate effective small- and large-core potentials to treat the core electrons of I atoms, and we include core−valence correlation effects in the large-core calculations. We use more extensive and optimized basis sets for the valence electrons of I atoms. In the previous study, we have employed bond functions to saturate the dispersion energy; however, as we will discuss later on, here, we remove them, and several extrapolation schemes are used and tested to extrapolate the interaction energies to CBS limit. One might consider adding this last item, as we realize that this might not improve reliability. In addition to reporting the new electronic structure computations, we present an analytic representation of the surface and new bound state calculations. Comparing the new bound-state results with the previous ones, as well as the experimental data, provides a test of the present surface.

Section II discusses (A) the details of the electronic structure calculations, (B) the analytical representation of the interaction potential (in particular, the fitting procedure to exactly reproduce the ab initio points), and (C) details and results of the bound-state calculations, together with their comparison to the experimental data. Section III contains some concluding remarks.

II. Computational Methods and Results

A. Ab Initio Electronic Structure Computations. All ab initio calculations are performed with the MOLPRO program,[22] by using the spin-restricted single and double excitations coupled cluster method with perturbative triples [RCCSD(T)] correlating only the valence electrons. We use Jacobi coordinates (r,R,θ) to describe the potential surface of HeI_2 complex, where R is the intermolecular distance of He atom from the center of mass of I_2, r is the bond length of I_2, and θ is the angle between the R and r vectors.

Scalar relativistic effects were accounted for by using relativistic ECPs for the I atoms. Two different ECPs have been compared: quasi-relativistic and relativistic large-core potentials denoted ECP46MWB[23] and ECP46MDF,[24] respectively, and a small-core potential denoted ECP28MDF.[25] The basis sets used in the large-core calculations have been optimized for the ECP46MWB by Martin and Sundermann[26] and for the ECP46MDF potential by Dolg.[24] The parameters for the ECP46MDF potential and the associated basis set are given in ref 20. For the small-core calculations, we used the augmented correlation consistent basis sets aug-cc-pVQZ-PP and aug-cc-pV5Z-PP optimized by Peterson et al.[27] For He, the corresponding aug-cc-pV(Q/5)Z basis sets[28] were used. In order to account for core−valence correlation effects, core polarization potentials (CPP)[29] were used in the large-core calculations, whereas core−core and core−valence correlation effects were entirely neglected in the small-core calculations.

The supermolecular method is used for the calculation of the interaction energies $\Delta E(r,R,\theta) = E_{HeI_2}(r,R,\theta) - E_{He} - E_{I_2}(r)$, and the counterpoise (CP) method[30] is used to correct for basis-set superposition errors (BSSE). Table 1 shows a comparison of RCCSD(T) interaction energies for small- and large-core ECP with different basis sets. For the small-core ECPs, a series of correlation consistent basis sets are available, and this allows us to extrapolate the energies to the (approximate) CBS limit. We have performed an extrapolation of the correlation energies by using three different extrapolation schemes. First, we utilized one of the most widely used, the mixed Gaussian/exponential three-point form proposed by Peterson et al.,[31] $E_X = E_{CBS} + Ae^{-(X-1)} + Be^{-(X-1)^2}$, where X is the cardinal number, and the series of aug-cc-pVTZ, aug-cc-pVQZ, and aug-cc-pV5Z basis sets was employed. Second, the two-point single inverse power function first introduced by Schwartz,[32] $E_X = E_{CBS} + A/X^3$, was applied by assuming the aug-cc-pVQZ and aug-cc-pV5Z basis sets. The extrapolated correlation energies were added to the aug-cc-pV5Z Hartree−Fock energies. The extrapolation was performed for all individual energies, and the CP corrected interaction energies were computed thereafter. At the end, we also used the two-point extrapolation scheme by using the inverse power series for both the BSSE-corrected and -uncorrected energies recently proposed by Lee et al.,[33] $E_{CBS} = (1/2)(\delta_X\varepsilon_{X+1} - \delta_{X+1}\varepsilon_X)/(\delta_X - \delta_{X+1})$, with $\delta_X = E_X^b - E_X^n$, $\varepsilon_X = E_X^b + E_X^n$. E^b is the energy corrected for BSSE, and E^I represents the uncorrected one. For this scheme, calculations require both

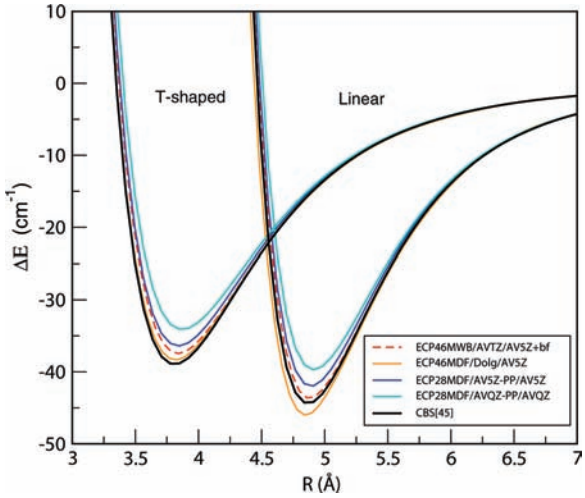

Figure 1. CCSD(T) interaction potentials for linear and T-shaped configurations for $r = 2.666$ Å obtained by using the indicated large-core or small-core ECPs and aug-cc-pV(Q/5)Z basis sets for I and He atoms, respectively. bf stands for a (3s3p2d2f1g) set of bond functions. CBS[45] extrapolated from AVQZ and AV5Z values (see text).

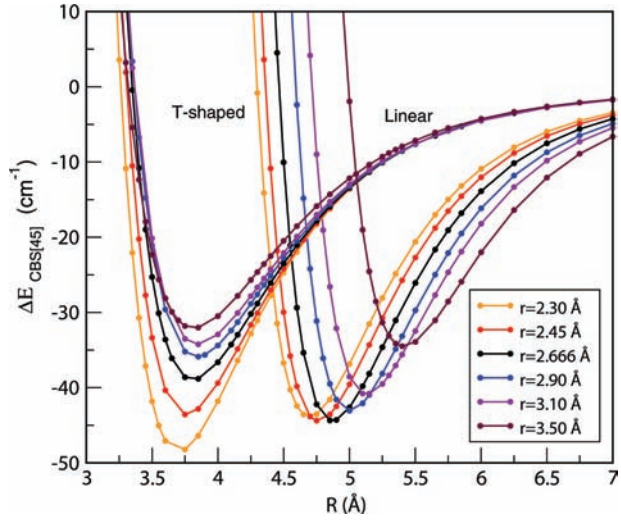

Figure 2. Dependence of the CBS[45] interaction energies for the linear and T-shaped configurations as r bond increases.

BSSE-corrected and -uncorrected energies, $E_X^b(r) = E_X^n + \Delta_{CP}$, where Δ_{CP} is the Boys−Bernardi CP correction to the energy. As it can be seen in Table 1, the extrapolated interaction energies of both two-point extrapolation schemes of the small-core calculations are in very good agreement with the relativistic large-core calculation, using aug-cc-pV5Z for He for the indicated configurations.

In Figure 1, we present the comparison for linear and T-shaped geometries of the RCCSD(T) potentials computed with large- and small-core ECPs, as well as their extrapolation to CBS[45] limit, obtained by the extrapolation form of ref 32. As we can see, the use of large-core ECPs predicts potential wells deeper than the ones computed with small-core ECPs, and in particular for the linear configurations, the well-depth values are even lower than the ones predicted by the CBS[45] scheme. Potential curves from previous calculations[12] obtained by using bond functions are also displayed. The CBS[45] interaction energies compare pretty well with the previous ones for the linear geometries, whereas differences for both the repulsive and attractive parts of the curve are found for the T-shaped configurations. For further comparison, computations performed by using the (3s3p2d2f1g) set of bond functions,[34] placed in the middle between He and the center of mass of I_2, were employed (see Table 1). In the present study, it appears that the use of the bond functions with both large- and small-core ECPS lead to a clear overestimation of the binding energy for the linear configurations, with a quite small effect on the T-shaped interaction energies. Therefore, they were not considered any further. Table 1 also shows MP4(SDTQ) calculations to estimate the contribution of quadruplet substitutions. In the current case, a rough estimate of nearly 0.5 cm^{-1} for the interaction energies was obtained.

On the basis of the above comparisons and the better CCSD(T) results obtained for the I_2 spectroscopic constants,[20] we decided to perform the final calculations by using the small-core ECP28MDF pseudopotentials together with the aug-cc-pVQ/5Z-PP basis sets for the I atoms[27] and the aug-cc-pVQ/5Z basis sets for the He. In turn, we applied the CBS[45] two-point extrapolation scheme[32] to obtain the interaction energies.

Intermolecular energies are calculated for 30−49 R distances ranging from $R = 2.60$ to 10 Å, and the angle θ is varied between 0 and 90° on a seven equally spaced (by 15°) grid, considering six different I_2 bond lengths with $r = 2.30$, 2.45, 2.666, 2.90, 3.10, and 3.50 Å. The r values are chosen around the equilibrium distance of $r_e = 2.666$ Å in a range that is enough to describe several excited vibrational levels (up to 50) of $I_2(X)$.

In Figure 2, we plot the ab initio CBS[45] interaction energies for $\theta = 0$ and 90° and for all the r values studied. We should note that small changes of r influence the overall interaction energy of the complex. In particular, for the smallest value $r = 2.30$ Å, the T-shaped configuration is found to be lower in energy than the linear one, whereas when the I—I bond is lengthened, the interaction energies for T-shaped geometries are found to be more sensitive than the linear ones. As can be seen, the interaction for the T-shaped configurations is predicted to become less attractive as r increases, whereas the interaction at linear configurations is much less affected. Therefore, for $r = 2.45$ Å, we found that the linear structures are lower in energy, with a difference of 0.8 cm^{-1}, than the T-shaped ones, and this energy difference increases for the next three r values studied. We should also mention that as r increases, the most attractive linear configurations are displaced at larger intermolecular distances R, whereas smaller displacements are found for the T-shaped ones.

B. Analytical Representation of the Potential Surface. In order to represent the potential energy surface for the HeI_2 complex, we used an analytical functional form to fit the CCSD(T) ab initio points. One common method is an expansion in Legendre polynomials, $P_\lambda(\cos\theta)$; thus, for He—I_2, we have

$$V(R,\theta;r_k) = \sum_\lambda V_{k\lambda}(R)\, P_\lambda(\cos\theta), \quad k = 1-6 \qquad (1)$$

with $\lambda = 0$, 2, 4, 6, 8, 10, 12 because of the symmetry of the system with respect to $\theta = 90°$, with the use of all seven angles to achieve convergence. The $V_{k\lambda}(R)$ coefficients are obtained by a collocation method applying the following procedure. After experimenting with various analytical expressions for obtaining a better adjustment of the ab initio data, we finally settled on a combination of a Morse-type form for the short-range part plus an extended vdW long-range part. Thus, for each of the seven values of angle θ and the six I_2 bond lengths r, we fitted the CCSD(T) data to the function,

$$V(R;\theta_i;r_k) = \alpha_0^{ik}(\exp(-2\alpha_1^{ik}(R-\alpha_2^{ik})) - 2\exp(-\alpha_1^{ik}(R-\alpha_2^{ik}))) - \frac{\alpha_3^{ik}}{R^6} - \frac{\alpha_4^{ik}}{R^8} - \frac{\alpha_5^{ik}}{R^{10}} - \frac{\alpha_6^{ik}}{R^{12}} \quad (2)$$

with parameters α_0^{ik}, α_1^{ik}, α_2^{ik}, α_3^{ik}, α_4^{ik}, α_5^{ik}, and α_6^{ik}, where $i = 1-7$ and $k = 1-6$. The resulting parameters listed in Table 2 are obtained by using a nonlinear least-squares fitting to the ab initio points. The model potential reproduces very well the ab initio values with a maximum standard deviation of 0.34 cm^{-1} and a total average standard deviation of 0.0445 cm^{-1} for all (r,R,θ) calculated values (see last column of Table 2). We should mention that, for linear and near-linear configurations, we obtained larger partial deviations compared to the T-shaped ones. This indicates that the analytical form represents better these interactions. For a three-dimensional representation of the potential, a one-dimensional cubic spline interpolation is employed for the r coordinate. In addition, the accuracy of the fit is checked by calculating some extra ab initio points (not included in the fitting procedure) along the minimum energy path (see circle points in Figure 3). In Table 3, we present, for the indicated geometries, the ab initio CCSD(T) energies, as well as their CBS[45] values, ΔE, and compare them with the corresponding $V(R,\theta;r_e)$ analytical ones. The latter points are found to have an average deviation of 0.045 cm^{-1} from original ab initio values.

TABLE 2: Parameters for the $V(R,\theta_i;r_k)_{i=1-7,k=1-6}$ Potential (eq 2) for HeI_2 Complex[a]

θ_i(deg)	α_0^{i1}	α_1^{i1}	α_2^{i1}	α_3^{i1}	α_4^{i1}	α_5^{i1}	α_6^{i1}	σ^{i1}
0	10.9241	1.81433	5.16916	516026	−7.794646(06)	−2.97034(08)	1.09254(10)	0.0602
15	15.8436	1.76541	5.06834	582585	−1.52098(07)	−1.30686(08)	7.42665(09)	0.0572
30	7.44512	1.63963	5.33771	648366	−3.07579(07)	5.45158(08)	−4.38756	0.0530
45	0.723548	1.60135	5.95848	294470	−4.58803(06)	1.45692(08)	1.11246(09)	0.0149
60	1.86147	1.555	5.47524	348450	−1.17862(07)	2.5981(08)	−6.09555(08)	0.0218
75	0.285405	1.58449	5.71753	248283	−4.32279(06)	1.15698(08)	−3.44007(08)	0.0118
90	1.32412	1.69042	4.90506	246957	−4.04617(06)	7.43335(07)	−1.94987(08)	0.0165
θ_i(deg)	α_0^{i2}	α_1^{i2}	α_2^{i2}	α_3^{i2}	α_4^{i2}	α_5^{i2}	α_6^{i2}	σ^{i2}
0	8.9736	1.79443	5.31764	591729	−1.12466(07)	−3.10233(08)	1.4317(10)	0.0737
15	16.7401	1.74795	5.14118	7091720	−2.28823(07)	−8.87488(07)	9.62302(09)	0.0741
30	0.0864152	1.61689	6.83894	531571	−2.32358(07)	7.5785(08)	1.00433	0.0441
45	0.905864	1.59366	5.94662	343371	−8.31253(06)	2.27953(08)	1.11616(09)	0.0200
60	17.8376	1.58865	4.66465	429921	−1.72786(07)	1.78366(08)	−1.72917	0.0402
75	2.07889	1.58276	5.09861	300591	−8.09287(06)	1.52784(08)	−4.42761(08)	0.0158
90	0.909432	1.65615	5.06133	243539	−3.70711(06)	7.13323(07)	−1.92577(08)	0.0168
θ_i(deg)	α_0^{i3}	α_1^{i3}	α_2^{i3}	α_3^{i3}	α_4^{i3}	α_5^{i3}	α_6^{i3}	σ^{i3}
0	8.8891	1.76195	5.43798	729124	−2.12023(07)	−1.20635(08)	1.60769(10)	0.0851
15	14.53	1.72365	5.30273	781053	−2.66887(07)	−1.0184(08)	1.33709(10)	0.0773
30	10.0882	1.64909	5.38554	699389	−2.91602(07)	2.47438(08)	6.04171(09)	0.0448
45	0.761746	1.58533	6.0803	376125	−1.00542(07)	2.74747(08)	1.77299(09)	0.0188
60	1.95732	1.5393	5.54267	395528	−1.50336(07)	3.35223(08)	−7.20145(08)	0.0175
75	1.61252	1.55803	5.2293	307342	−8.44853(06)	1.67713(08)	−5.04678(08)	0.0133
90	1.27045	1.62092	4.98674	247708	−3.87654(06)	6.80205(07)	−1.84884(08)	0.0145
θ_i	α_0^{i4}	α_1^{i4}	α_2^{i4}	α_3^{i4}	α_4^{i4}	α_5^{i4}	α_6^{i4}	σ^{i4}
0	12.9961	1.74166	5.44919	797671	−2.08375(07)	−4.73419(08)	2.4222(10)	0.0905
15	13.1626	1.69201	5.46721	914595	−3.67805(07)	3.11571(07)	1.71621(10)	0.0793
30	0.0927259	1.57751	7.08433	816966	−4.83924(07)	1.49904(09)	1.03505	0.0606
45	1.72319	1.57373	5.89559	437983	−1.43222(07)	3.07378(08)	2.6036(09)	0.0214
60	1.17251	1.51461	5.79	416270	−1.68336(07)	4.20949(08)	−1.06585(09)	0.0191
75	3.19769	1.54427	5.01724	335357	−1.05377(07)	1.86128(08)	−5.5897(08)	0.0134
90	2.44893	1.59684	4.77794	258932	−4.61293(06)	6.79736(07)	−1.82422(08)	0.0135
θ_i(deg)	α_0^{i5}	α_1^{i5}	α_2^{i5}	α_3^{i5}	α_4^{i5}	α_5^{i5}	α_6^{i5}	σ^{i5}
0	14.1962	1.72826	5.54241	692450	−1.18736(06)	−1.5691(09)	4.34721(10)	0.0838
15	11.6008	1.66462	5.63095	1.03946(06)	−4.67573(07)	1.20999(08)	2.32582(10)	0.0937
30	18.3149	1.62446	5.39556	924536	−4.1903(07)	−2.89101(07)	1.56084(10)	0.0695
45	13.0148	1.58083	5.263	612426	−2.62257(07)	1.69879(08)	4.67689(09)	0.0617
60	1.12255	1.4958	5.8608	441838	−1.91826(07)	4.91875(08)	−1.34986(09)	0.0246
75	2.99533	1.52676	5.0497	331660	−1.02312(07)	1.8178(08)	−5.5206(08)	0.0126
90	1.77983	1.56627	4.88096	244049	−3.63468(06)	5.3854(07)	−1.44496(08)	0.0205
θ_i(deg)	α_0^{i6}	α_1^{i6}	α_2^{i6}	α_3^{i6}	α_4^{i6}	α_5^{i6}	α_6^{i6}	σ^{i6}
0	13.5592	1.67562	5.79126	841001	−1.25962(07)	−1.74207(09)	6.07437(10)	0.0873
15	18.6434	1.62905	5.70331	1.18116(06)	−5.21037(07)	−7.81914(08)	4.81181(10)	0.1021
30	0.0211224	1.51535	7.94872	1.22924(06)	−9.57486(07)	3.15023(09)	1.00406	0.0904
45	9.7246	1.50578	5.56409	930032	−6.23447(07)	1.20026(09)	1.0014	0.0673
60	4.15693	1.47819	5.45476	507620	−2.57387(07)	5.45628(08)	−1.34705(09)	0.0244
75	2.6833	1.49076	5.08549	297667	−8.36097(06)	1.50748(08)	−4.60223(08)	0.0160
90	2.94578	1.52588	4.65638	229683	−3.33962(06)	3.87548(07)	−9.74171(07)	0.0252

[a] σ^{ik} is the partial average standard deviation for each θ_i and r_k values. Distances are in Å and energies in cm^{-1}. Figures in parentheses are powers of 10.

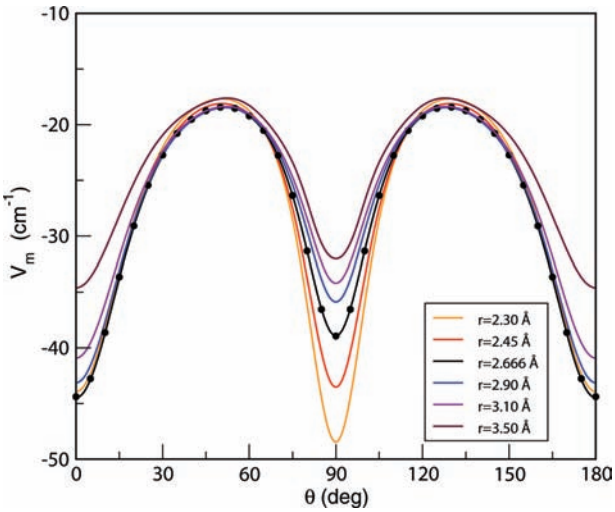

Figure 3. Minimum energy, V_m in cm^{-1} (eq 1), as a function of angle θ and bond-length r. Filled circles are for the ab initio points listed in Table 3.

The potential minima and the corresponding barrier are displayed in Figure 3, where the minimum energy path, V_m, values are plotted as a function of the angle θ and the bond length r. As it has been mentioned above, the T-shaped minimum is displaced to $r \approx 2.30$ Å, whereas the linear one is remaining close to $r = r_e = 2.666$ Å in the three-dimensional surface. For the equilibrium I—I bond distance, r_e, the global minimum with an energy of -44.28 cm^{-1} at $R = 4.828$ Å corresponds to a linear ($\theta = 0°$) configuration, whereas the second minimum, with energy of -38.92 cm^{-1}, is at $R = 3.818$ Å and corresponds to a T-shaped ($\theta = 90°$) configuration of the complex. The isomerization barrier between the two wells is found at an energy of -18.42 cm^{-1} (25.86 cm^{-1} above the global linear minimum), with $R = 4.89$ Å and $\theta \approx 51°$. The present calculations predict a slightly smaller (5.36 cm^{-1}) difference between the energies of the two structures at $r = 2.666$ Å than the previous CCSD(T) results.[12]

Previous ab initio calculations for the HeI_2 ground-state potential at MR CISD[11] and CCSD(T)[12] levels of theory have also predicted a two-well topology, with the linear one being the deepest one. However, in the earlier study, significantly shallower well depths have been estimated for both the linear and T-shaped configurations with values of -26.37 and -24.12 cm^{-1}, respectively, compared to the CCSD(T) results of -43.25 and -37.32 cm^{-1}. Unfortunately, no more theoretical attempts are available in the literature. The estimate of the experimental value of D_e given by Levy and co-workers[7] for the perpendicular structure of HeI_2 was 21.6−22.7 cm^{-1}, whereas a study on atom−diatomic molecule collinear collisions has predicted[35] a well depth of ground HeI_2 of -52.10 cm^{-1}. More recently, Loomis and co-workers[6] have proposed D_e values of -45.24 and -40.00 cm^{-1} for linear and T-shaped minimum, respectively. These well depths have been estimated by scaling the previous ab initio surface[12] in order to provide the experimental binding energies for both conformers. As we can see, the well-depth estimates of the present study are very close to these latter values.

C. Bound-State Calculations and Comparison with Experiment. The rovibrational Hamiltonian in the Jacobi coordinate system has the form

$$\hat{H} = -\frac{\hbar^2}{2\mu_1}\frac{\partial^2}{\partial R^2} + \frac{\hat{j}^2}{2\mu_2 r^2} + \frac{\hat{l}^2}{2\mu_1 R^2} + V(R,\theta,r) + \hat{H}_{I_2} \quad (3)$$

where $\hat{H}_{I_2} = -\hbar^2/(2\mu_2)(\partial^2/\partial r^2) + V_{I_2}(r)$ is the vibrational Hamiltonian for a free I_2 molecule and $V_{I_2}(r)$ is the I_2 ground-state potential calculated by using the CBS[45] extrapolation scheme, as described above in Section II.A. $1/\mu_1 = 1/m_{He} + 1/(2m_I)$ and $1/\mu_2 = 1/m_I + 1/m_I$ are the reduced masses, $m_{He} = 4.00260$ and $m_I = 126.904473$ amu are the atomic masses of ^{4}He and ^{127}I isotopes, and $\hat{l}$ and $\hat{j}$ are the angular momentum operators associated with the vectors R and r, respectively, leading to a total angular momentum $\hat{J} = \hat{l} + \hat{j}$.

As in earlier work,[12] the bound vdW levels and corresponding wave functions are calculated variationally by diagonalizing the two-dimensional, with r fixed 2.666 Å, or the vibrationally averaged Hamiltonian. Figure 4 presents a two-dimensional contour plot of the vibrationally averaged $V_{v,v}(R,\theta) = \langle\chi_v|V(R,\theta,r)|\chi_v\rangle$ potential for $v = 0$, in the (θ,R) plane. The surface has minima for linear and T-shaped configurations. In addition, here, because of the small difference in the binding energies of the two conformers and in order to minimize errors, we used various vibrational basis functions, $\chi_v(r)$, in the vibrational three-dimensional calculations ($J = 0$).

In short, the Hamiltonian is represented on a finite three-dimensional basis set, and the resulting generalized eigenvalue problem is then solved by using routines from the Lapack Library.[36] The $V_{v,v'}$ potential matrix elements are calculated, for v values in the range [0−2], by using 61-points Gaussian quadrature in the r coordinate for $r = 2.2$−.4 Å. For the angular coordinate, we used orthonormalized Legendre polynomials $\{P_j(\cos\theta)\}$ as basis functions, with up to 48 and 49 values, for even and odd symmetry, respectively, of the diatomic rotation j. For the radial R coordinate, a discrete variable representation (DVR) basis set is used based on the particle in a box eigenfunctions.[37] A basis set of 140 DVR functions over the range from $R = 2.85$ to 12.0 Å is used. In this way, a convergence of 0.0005 cm^{-1} is achieved in bound-state calculations.

The energies of the lowest-energy vdW levels of calculations are listed in Table 4, together with data from previous studies.[6,12] As it can be seen, all computations show that the two lowest vdW levels correspond to linear configurations, and the next one corresponds to the T-shaped one, with an energy difference of 0.186, 0.206, and 0.208 cm^{-1}, respectively. Comparison with results of the previous surface shows that the binding energies of the two isomers are lower in the new surface (see columns 1 and 2 in Table 4). As it was expected from the ab initio computations, the energy of the T-shaped state is more affected than the linear one, when comparing them with the ones obtained by using the previous surface.[12] Also, we found that there is no effect on the energy levels in the three-dimensional bound-state calculation. Figure 5b presents the minimum energy path for the vibrationally average potential for $v = 0$ value. The averaged potentials curves for v values up to 7 are found to be very similar to each other, with very small changes around the wells for the linear and T-shaped configurations. We should also mention that the energy difference of the two isomers is very close to the value of the maximum partial averaged standard deviation (0.1 cm^{-1}) obtained in the fitting procedure. This indicates that the present potential surface predicts a relative stability of the two isomers within its uncertainty with respect to the original ab initio data.

The vibrational levels ($n = 0,1,2$) are at energies of -15.717 (even), -15.717 (odd), and -15.509 (even) cm^{-1}, and the

TABLE 3: CCSD(T), CBS[45] Interaction Energies, ΔE (See Text), and Potential $V(R,\theta;r_e)$ (See Eq 1) Values along to the Minimum Energy Path for The HeI_2 Complex[a]

(θ, R)	CCSD(T)/AVQZ	CCSD(T)/AV5Z	CBS[45]	V(θ,R;r_e)	$E_{CBS[45]}$-V
(0,4.87)	−39.49	−41.94	−44.40	−44.48	0.082
(5,4.88)	−37.97	−40.36	−42.77	−42.85	0.080
(10,4.93)	−34.37	−36.48	−38.63	−38.73	0.102
(15,4.98)	−29.88	−31.74	−33.65	−33.75	0.104
(20,5.03)	−25.76	−27.39	−29.09	−29.16	0.074
(25,5.07)	−22.49	−23.93	−25.45	−25.50	0.052
(30,5.09)	−20.07	−21.37	−22.73	−22.78	0.049
(35,5.08)	−18.34	−19.54	−20.80	−20.86	0.061
(40,5.05)	−17.19	−18.33	−19.53	−19.56	0.026
(45,4.99)	−16.47	−17.59	−18.75	−18.77	0.016
(50,4.92)	−16.20	−17.30	−18.43	−18.43	0.0002
(55,4.82)	−16.30	−17.41	−18.55	−18.56	0.005
(60,4.69)	−16.82	−17.99	−19.21	−19.21	−0.002
(65,4.55)	−17.99	−19.23	−20.52	−20.56	0.042
(70,4.38)	−19.94	−21.33	−22.78	−22.83	0.047
(75,4.20)	−23.06	−24.67	−26.37	−26.36	−0.010
(85,3.87)	−31.81	−34.12	−36.56	−36.52	−0.040
(90,3.81)	−33.83	−36.32	−38.94	−38.93	−0.015

[a] Energies are in cm^{-1}, angles are in degrees, and distances are in Å.

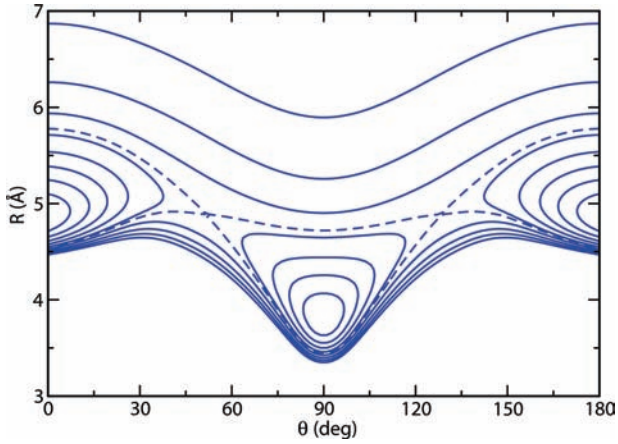

Figure 4. Contour plots of the vibrationally averaged $V_{v,v}(R,\theta)$ potential for $v = 0$, in the (θ,R) plane. Contour intervals are of 5 cm^{-1} and for energies from −40 to 0 cm^{-1}. The dashed line corresponds to the energy of −18.43 cm^{-1} of the isomeriazation barrier.

TABLE 4: Energies for the Indicated Bound Vibrational vdW Levels of HeI_2 (X)

n	this work, (2D)/ ($v = 0$)/(3D)	unscaled PES[12], ($v = 0$)	scaled PES[6]/Expt.[6]
0	−15.738/−15.713/−15.717	−15.38	−16.59/−16.6(6)
1	−15.738/−15.713/−15.717	−15.38	−16.33/−16.3(6)
2	−15.552/−15.507/−15.509	−14.68	−16.33/−16.3(6)
3	−8.305/−8.300/−8.300	−7.97	−8.97/
4	−7.527/−7.526/−7.527	−7.26	−8.04
5	−6.441/−6.438/−6.439	−6.12	−7.03
6	−4.618/−4.617/−4.618	−4.34	−5.24
7	−1.994/−1.998/−1.999		

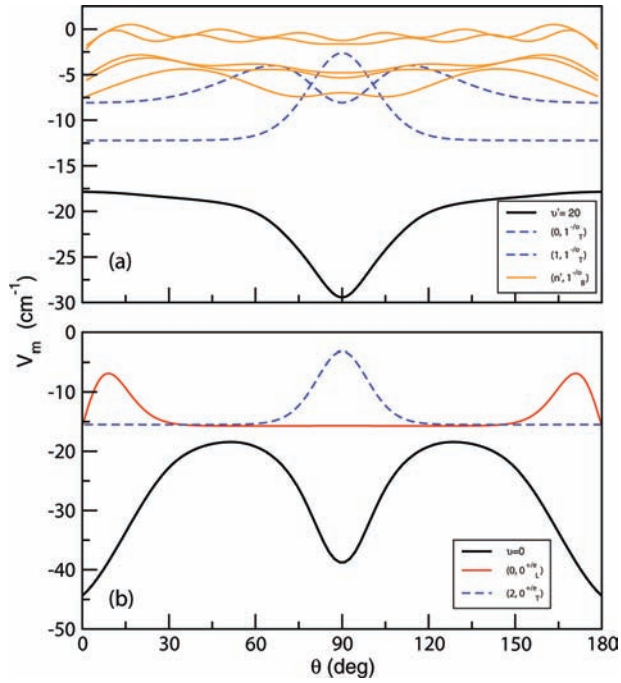

Figure 5. Minimum energy path of the vibrationally averaged $V_{v,v}$ potentials, for (a) He—I_2 (B, $v' = 20$) and (b) He sbdI_2 (X, $v = 0$) as a function of angle θ. The angular probability distributions of the two lowest-energy intermolecular vdW levels with $J = 0$ ($p = +1$, $j =$ even) for the X surface and $J' = 1$ ($p' = -1$, $j' =$ odd) for the B one are superimposed. For each eigenstate, the zero probability corresponds to its energy value. Solid (orange) lines indicate bent/free-rotor states, where $n' \geq 2$ (a), solid (red) line is for the state localized in the linear well (b), and dashed lines correspond to the ones localized in T-shaped wells (a,b).

associated wave functions correspond to linear configurations for the first two states and to T-shaped configurations for the last one (see Figure 5b). The next four vibrational states are found at energies of −8.300, −7.527, −6.439, and −4.618 cm^{-1} and are spreading over all θ values. All calculated vdW vibrational levels are located above the potential isomerization barrier, whereas the first three are below the barrier of the effective potential. The small energy difference between $n =$ 0, 1 and $n = 2$ states (only 0.2 cm^{-1}) provides indications for coexistence of the two isomers at as low temperatures as 0.29 K. Vibrationally averaged structures with $R_0 = 5.34$ Å and $R_0 = 4.36$ Å are obtained for the linear and T-shaped isomers, respectively. Analysis of the rotational structure of the B ← X spectrum[38] indicated a perpendicular structure with $R_0 = 4.47 \pm 0.13$ Å for the X state, which is in very good accord with the T-shaped one predicted in the present work (see Table 5).

In Table 5, we also compare the results obtained with the present CCSD(T) surface with previous theoretical and experimental data available. The experimental value for binding energy of the ground T-shaped HeI_2 has been first determined[7] to be in the range between 18.2 and 19.4 cm^{-1}, and a revised value of 17.6 ± 1.0 cm^{-1} has been later proposed,[8] based on accurate

TABLE 5: Experimental and Theoretical Binding Energies (D_e and D_0 in cm^{-1}) and Equilibrium Distances (R_e and R_0 in Å) for the Linear and T-Shaped Isomers of the He−I_2 Complex

	linear He−I_2			T-shaped He−I_2		
	D_e[a]	D_0	R_e[a]/R_0	D_e[a]	D_0	R_e[a]/R_0
this work	44.28	15.72	4.83/5.34	38.92	15.51	3.82/4.36
ab initio CCSD(T) value[12]	43.52	15.38	4.89/5.34	37.32	14.68	3.84/4.40
ab initio MR CISD value[b]	26.37		5.03/-	24.12		3.97/-
semiempirical value[c]	52.1	33.1	4.24/-			
experimental value[7]				22.15 ± 0.55	18.8 ± 0.6	3.94/4.47
experimental value[8]					17.6 ± 1.0	
experimental value[6]	45.24[d]	16.3 ± 0.6	4.89[d]	40.00[d]	16.6 ± 0.6	3.84[d]

[a] Potential well depth and equilibrium distance values from $V(R,\theta,r = 2.666Å)$, see eq 1. [b] Lowest interaction energies for linear and T-shaped configurations of HeI_2 given in ref 11. [c] Potential parameters for studying atom−diatomic molecule collinear collisions from ref 35. [d] Potential well depths and equilibrium distances given in ref 6. These values have been obtained by scaling the previous CCSD(T) surface[12] to reproduce the experimental binding energies of each isomer.

TABLE 6: Comparison with Previous Available Theoretical Blue-Shift Values and Experimental and Theoretical Energies in cm^{-1} for the HeI_2 (B, $v' = 20$) vdW Levels for $J = 1$, Together with Spectral Blue-Shift Values for the Indicated HeI_2 (B, $v' = 20, n', Jp', j'$) ← (X, $v = 0, n, J^p, j$) Transitions[a]

	$E_{HeI_2(B,v'=20,n')}$		(B, $v' = 20$) ← (X, $v = 0$) blue shift		
n', J^p_C	scaled PES[6]	CCSD(T) PES[21]	theor.[6b]	theor.[21c]	this work[d]
$0,0^+_T$	−16.10	−12.35	0.49	2.33	3.16
$1,0^+_T$	−9.46	−8.27	7.14	6.41	7.24
$2,0^+_B$	−7.65	−7.64	8.94/8.68	7.04/7.74	7.87/8.08
$3,0^+_B$	−6.75	−6.83	9.84/9.58	7.85/8.55	8.68/8.89
$4,0^+_B$	−5.80	−5.86	10.79/10.53	8.82/9.52	9.65/9.86
$5,0^+_B$	−4.24	−4.24	12.35/12.09	10.44/11.14	11.27/11.48
$6,0^+_B$	−2.67	−2.57	13.92/13.66	12.11/12.81	12.94/13.15

	expt.[6]	this work (j' = o/e)	transition (n',J^p,j') ← (n,J^p,j)	this work	expt.[e]
$0,1^-_T$	−12.8	−12.32/−12.12	(0,1 $^-$, o) ← (2,0 $^+$, e)	3.19	3.8
$1,1^-_T$	.	−8.08/−8.35	(1,1$^-$, o) ← (2,0$^+$, e)	7.44	
$2,1^-_B$	−7.9	−7.54/−7.02	(2,1$^-$, o) ← (2,0$^+$, e)/(0,0$^+$, e)	7.97/8.18	8.7/8.4
			(2,1$^-$, e) ← (1,0$^+$, o)	8.70	
$3,1^-_B$	−6.8	−5.88/−6.71	(3,1$^-$, o) ← (2,0$^+$, e)/(0,0$^+$, e)	9.63/9.84	9.8/9.5
			(3,1$^-$, e) ← (1,0$^+$, o)	9.01	
$4,1^-_B$	−5.7	−5.49/−4.43	(4,1$^-$, o) ← (2,0$^+$, e)/(0,0$^+$, e)	10.02/10.23	10.9/10.6
			(4,1$^-$, e) ← (1,0$^+$, o)	11.29	
$5,1^-_B$	−4.2	−2.68/−3.93	(5,1$^-$, o) ← (2,0$^+$, e)/(0,0$^+$, e)	12.84/13.05	12.4/12.1
			(5,1$^-$, e) ← (1,0$^+$, o)	11.79	
$6,1^-_B$	−2.2	−2.10/−0.86	(6,1$^-$, o) ← (2,0$^+$, e)/(0,0$^+$, e)	13.42/13.62	14.4/14.1
			(6,1$^-$, e) ← (1,0$^+$, o)	14.86	

[a] Computed blue shifts are obtained by using both $D_0^T(X,v = 0,n = 2)/D_0^L(X,v = 0,n = 0)$ energies for the $n' \geq 2$ states (see text). [b] Blue-shift values calculated from the theoretical scaled PES and experimental data of $E_{HeI_2(B,v'=20,n'=0-6)}$ and $D_0(X,v = 0,n = 0-2)$ (see Tables 1, 2, and 3 in ref 6). [c] Blue-shift values calculated from the theoretical data of $E_{HeI_2(B,v'=20,n'=0-6)}$ (see Table 4 in ref 21 and $D_0(X,v = 0,n = 0-2)$ (see Table 5 in ref 12). [d] $E_{HeI_2(B,v'=20,n'=0-6)}$ values (see third column) from ref 21are used. [e] Blue-shift values calculated from the theoretical scaled PES and experimental data of $E_{HeI_2(B,v'=20,n'=0-6)}$ and $D_0(X,v = 0,n = 0-2)$ (see Tables 1, 2, and 3 in ref 6).

values for the blueshifts of the HeI_2 B ← X excitation spectra.[9] Recently, Loomis and co-workers[6] have reported binding-energy values for both T-shaped and linear isomers to be 16.6 ± 0.6 and 16.3 ± 0.6 cm^{-1}, respectively. We should note that the new surface predicts, in excellent agreement with the experiment, the existence of the two isomers, although with the reverse ordering. Our estimates of 15.51 and 15.72 cm^{-1} for the D_0 binding energies are very close to each other and close to the lower bound of the later experimental values (see Table 5).

Direct experimental data are available only for the D_0 value of the HeI_2 B state and the spectral blue-shift value with respect the corresponding band of the uncomplexed iodine molecule.[6,9,39] The blue shifts correspond to the difference between the dissociation energies of the initial and final states of the transition, $D_0(B,v',n') - D_0(X,v = 0,n)$. In the top panel of Table 6, we listed the blue-shift values obtained here, as the difference of the $D_0(B,v' = 20,n' = 0-6) - D_0(X,v = 0,n = 0-2)$ and compare them with the ones available from previous theoretical calculations for = 0.[6,21] The energy levels are labeled as J^p_C, where J is the total angular momentum, p is the parity under total nuclear coordinates inversion (+1 for even, −1 for odd), and C being L, T, and B, for linear, T-shaped, and bent configurations, respectively. By taking into account the Franck−Condon factors, that strongly favor the transition between the T-shaped $n' = 0,1$ and $n = 2$ vdW levels (see Figure 6 in ref 20 and Figure 5b), values of 3.16 and 7.24 cm^{-1} are predicted, whereas for $n' > 2$, both transitions from ground-state T-shaped and linear vdW levels are obtained (see last column of Table 6) for the $J = 0$ energies. As we can see (in the fifth column), smaller values by 0.83 and 0.34 cm^{-1} are obtained for all transitions from the T-shaped and linear ground-state isomers, respectively, compared to the previous calculations,[21] where the previous X state potential has been employed.[12] In the forth column of Table 6, we also present results from previous theoretical spectra calculations of the HeI_2 in the B−X, 20−0 region.[6] We should mention that in the above-

mentioned study, states with $J \leq 9$ on X and B surfaces have been calculated, and theoretical simulations, as well as comparison with the experimental observed spectra, have been carried out. Here, we compare with the results available for $J = 0$ (see Tables 2 and 3 in ref 6) by using a scaled version of our previous CCSD(T) X-state surface and a scaled pairwise B-state potential. One can see that, for all $n' \geq 1$, the agreement is good, whereas the larger difference obtained for the $n' = 0$ is due to the B-state potential used in that work.[6]

However, we should note that in order to compare with the experimental values more accurately, one should consider the selection rules for dipole allowed transitions ($\Delta J = 0, \pm 1$, $0 \not\leftrightarrow 0$, $p \neq p'$), including several J values in the calculations. Here, by using the B-state potential energy surface of ref 20, we carried out calculations for the vdW levels of HeI_2 ($B,v' = 20,n'$) for $J' = 1$ and $p' = -1$. Details on the metholology for the $J' > 0$ calulations are given in refs 14 and 15. A basis set of 100 DVR functions over the range from $R = 2$ to 12 Å and up to 25 values of the diatomic rotation j' *are use*d. The results for the $n' = 0-6$ (with $j' =$ odd/even) levels, as well the experimental values stemming from Table 3 of Ray et al.,[6] are reported in Table 6, and angular distributions of the corresponding ($J' = 1$ and $p' = -1$, $j' =$ odd) eigenfunctions are plotted together with the vibrationally averaged ($B,v' = 20$) potential in Figure 5a. As in Figure 5b, the probability values of the wave functions were shifted in such a way that the zero amplitude for each of them corresponds to its energy value. As seen in Figure 5a, only the first two vdW levels are mainly localized in the T-shaped well, whereas the wave functions of the next states are delocalized and are spreading over all angle values θ, with large amplitude for near-linear configurations. As a result, these states have significant overlaps with the linear X-state isomer (see Figure 5b) and contribute to the features of the experimental spectrum. The blue shifts listed in Table 6 are calculated as the difference between the dissociation energies of the initial and final states of the transition, $D_0(B,v' = 20,n') - D_0(X,v = 0,n)$, by taking into account the above-mentioned selection rules in the theoretical computations. On the basis of the localization patterns (see Figure 5a,b), the $n' = 0$ and 1 levels give rise to transitions to the ground T-shaped ($n = 2$) state, whereas the higher n' states could contribute to transitions to both (linear and T-shaped) ground vdW levels. Therefore, in Table 6, we present both blue-shift values and compare them with the ones obtained from the experimental values listed in Tables 1 and 3 in ref 6. Ray et al. also provide in their Figure 7a the excited band spectrum recorded between 8.5 and 14 cm^{-1}, shifted from the I_2 band origin, where four main peaks can be seen in this range, with the first one being located at 9.3−9.4 cm^{-1}. We should note that experimental data includes various J values, whereas for the theoretical blue shifts, we count only with allowed transitions ($J' = 1 \leftarrow J = 0$), and these values extend from 8.0 cm^{-1} for $n' = 2$ to 14.9 cm^{-1} for $n' = 6$. As we can see in Table 6, the agreement with the experimental values is remarkable for both T-shaped and linear features, with a difference of only 0.6 cm^{-1} for $n' = 0$, that, is just within the experimental uncertainty.

III. Conclusions

We reported a new, extended CCSD(T) ab initio calculations of HeI_2 interaction in the ground electronic state, including the dependence of both I_2 orientation and vibrational displacement. Relativistic effects are included with the use of ECPs for I atoms, together with large consistent correlated basis sets. In turn, interaction energies are extrapolated at their (approximate) CBS limit by employing different extrapolation schemes.

We implemented an analytic representation for the interaction potential of the HeI_2 (X) complex. The new functional form reproduces very well all ab initio data, with partial averaged deviations of 0.1 cm^{-1}, and in particular the ones nearby the T-shaped configurations, with partial averaged deviations of less than 0.05 cm^{-1}.

We performed vibrational bound-state calculations to compute the vdW states of the ground HeI_2 complex. The isomer corresponding to a He—I—I linear configuration is predicted to be the most stable with a binding energy of 15.72 cm^{-1}, whereas the T-shaped isomer is found to lie only 0.2 cm^{-1} above, indicating their coexistence even at low temperatures. The above values are in excellent agreement with recent experimental observations by Loomis's group,[6] the discrepancy being at most 1.0 cm^{-1} with the experimental uncertainty of 0.6 cm^{-1}. The agreement is almost remarkable, when taking into account that no adjustment is made on the potential surface with respect to the experiments. Although the new interaction potential is based on state-of-the-art ab initio electronic structure calculations and a faithful analytic representation, the bound-state calculations using it still do not exactly account for recent experimental measurements. This is due to the necessity of different fitting procedure and/or more ab initio data in determining the analytic representation and to deficiencies in calculations. The difference of nearly 1 cm^{-1} from the experimental measurements may be attributed to the level of theory and convergence in ab initio computations. For selected configurations, we evaluate the effect of the quadruple substitutions at MP4 level; however, for a more accurate description, more sophisticated and computationally more expensive methods, such as renormalized CCSD(T), CCSD(TQ),[40] or even CCSDT(Q)[41] ones, should be employed.

Experimental information available in combination with first-principle theoretical calculations for such complexes could provide reliable potential-energy surfaces for interpreting their dynamics. Such accurate interaction potentials are also demanded for studying collisions of molecules with ultracold rare-gas atoms in optical traps,[42] as well as spectroscopy of larger rare-gas−dihalogen clusters,[17,18,43] where a diatomic molecule interacts with a solvent system of rare-gas atoms.[43−45] In this vein, it is clear that experimental studies similar to those reported recently[46] on the spectroscopic identification of such higher-order rare-gas−dihalogen complexes, in combination with theoretical predictions, are invaluable for understanding the nature of the underlying intermolecular forces.

Acknowledgment. The authors thank to Centro de Calculo (IFF), CTI (CSIC), CESGA, and GSC (CIEMAT) for allocation of computer time. L.G.-G. acknowledges CSIC for the "Introducción a la investigación" fellowship. This work has been supported by DGICYT, Spain, Grant no FIS2007-62002.

References and Notes

(1) Buchachenko, A. A.; Prosmiti, R.; Cuhna, C.; Villarreal, P.; Delgado-Barrio, G. *J. Chem. Phys.* **2002**, *117*, 6117.
(2) Boucher, D. S.; Bradke, M. D.; Darr, J. P.; Loomis, R. A. *J. Phys. Chem. A* **2003**, *107*, 6901.
(3) Darr, J. P.; Loomis, R. A.; McCoy, A. B. *J. Chem. Phys.* **2004**, *120*, 2677.
(4) Darr, J. P.; Clennon, J. J.; Loomis, R. A. *J. Chem. Phys.* **2005**, *122*, 131101.
(5) Pio, J. M.; van der Veer, W. E.; Bieler, C. R.; Janda, K. C. *J. Chem. Phys.* **2008**, *128*, 134311.
(6) Ray, S. E.; McCoy, A. B.; Glennon, J. J.; Darr, J. P.; Fesser, E. J.; Lancaster, J. R.; Loomis, R. A. *J. Chem. Phys.* **2006**, *125*, 164314.
(7) Blazy, J. A.; DeKoven, B. M.; Russell, T. D.; Levy, D. H. *J. Chem. Phys.* **1980**, *72*, 2439.
(8) Jahn, D. G.; Clement, S. G.; Janda, K. C. *J. Chem. Phys.* **1994**, *101*, 283.

(9) Sharfin, W.; Kroger, P.; Wallace, S. C. *Chem. Phys. Lett.* **1982**, *85*, 81.
(10) Schwenke, D. W.; Truhlar, D. G. *Chem. Phys. Lett.* **1983**, *98*, 217.
(11) Brown, F. B.; Schwenke, D. W.; Truhlar, D. G. *Theor. Chim. Acta* **1985**, *68*, 23.
(12) Prosmiti, R.; Valdés, A.; Villarreal, P.; Delgado-Barrio, G. *J. Phys. Chem. A* **2004**, *108*, 6065.
(13) Prosmiti, R.; Villarreal, P.; Delgado-Barrio, G. *Chem. Phys. Lett.* **2002**, *359*, 473.
(14) Valdés, A.; Prosmiti, R.; Villarreal, P.; Delgado-Barrio, G. *Chem. Phys. Lett.* **2003**, *357*, 328.
(15) Prosmiti, R.; Cunha, C.; Villarreal, P.; Delgado-Barrio, G. *J. Chem. Phys.* **2003**, *119*, 4216.
(16) Valdés, A.; Prosmiti, R.; Villarreal, P.; Delgado-Barrio, G. *Mol. Phys.* **2004**, *102*, 2277.
(17) Valdés, A.; Prosmiti, R.; Villarreal, P.; Delgado-Barrio, G. *J. Chem. Phys.* **2005**, *122*, 044305.
(18) Valdés, A.; Prosmiti, R.; Villarreal, P.; Delgado-Barrio, G. *J. Chem. Phys.* **2006**, *125*, 014313.
(19) Diez-Pardos, C.; Valdés, A.; Prosmiti, R.; Villarreal, P.; Delgado-Barrio, G. *Theor. Chem. Acc.* **2007**, *118*, 511.
(20) Valdés, A.; Prosmiti, R.; Villarreal, P.; Delgado-Barrio, G.; Werner, H.-J. *J. Chem. Phys.* **2007**, *126*, 204301.
(21) Valdés, A.; Prosmiti, R.; Villarreal, P.; Delgado-Barrio, G.; Lemoine, D.; Lepetit, B. *J. Chem. Phys.* **2007**, *126*, 244314.
(22) Werner, H.-J.; Knowles, P. J.; Schtz, M.; Lindh, R.; Celani, P.; Korona, T.; Rauhut, G.; Manby, F. R.; Amos, R. D.; Bernhardsson, A.; Berning, A.; Cooper, D. L.; Deegan, M. J. O.; Dobbyn, A. J.; Eckert, F.; Hampel, C.; Hetzer, G.; Lloyd, A. W.; McNicholas, S. J.; Meyer, W.; Mura, M. E.; Nickla, A.; Palmieri, P.; Pitzer, R.; Schumann, U.; Stoll, H.; Stone, A. J.; Tarroni, R.; Thorsteinsson, T. *MOLPRO, version 2006.1, a package of ab initio programs*; Birmingham, UK, 2006.
(23) Bergner, A.; Dolg, M.; Kuechle, W.; Stoll, H.; Preuss, H. *Mol. Phys.* **1993**, *80*, 1431.
(24) Dolg, M. Habilitationsschrift, Universität Stuttgart, 1997.
(25) Peterson, K. A.; Figgen, D.; Goll, E.; Stoll, H.; Dolg, M. *J. Chem. Phys.* **2003**, *119*, 11113.
(26) Martin, J. M. L.; Sundermann, A. *J. Chem. Phys.* **2001**, *114*, 3408.
(27) Peterson, K. A.; Figgen, D.; Goll, E.; Stoll, H.; Dolg, M. *J. Chem. Phys.* **2003**, *119*, 11113.
(28) Kendall, R. A.; Dunning, T. H., Jr.; Harrison, R. J. *J. Chem. Phys.* **1992**, *96*, 6796.
(29) Müller, W.; Flesch, J.; Meyer, W. *J. Chem. Phys.* **1984**, *80*, 3297.
(30) Boys, S. F.; Bernardi, F. *Mol. Phys.* **1970**, *19*, 553.
(31) Peterson, K. A.; Woon, D. E.; Dunning, T. H., Jr. *J. Chem. Phys.* **1994**, *100*, 7410.
(32) Schwartz, C. *Phys. Rev.* **1962**, *126*, 1015.
(33) Lee, E. C.; Kim, D.; Jurecka, P.; Tarakeshwar, P.; Horza, P.; Kim, K. S. *J. Phys. Chem. A* **2007**, *111*, 3446.
(34) Cybulski, S. M.; Toczylowski, R. R. *J. Chem. Phys.* **1999**, *111*, 10520.
(35) Secrest, D.; Eastes, W. *J. Chem. Phys.* **1972**, *56*, 2502.
(36) http://www.netlib.org/lapack/, http://www.intel.com.
(37) Muckerman, J. T. *Chem. Phys. Lett.* **1990**, *173*, 200.
(38) Smalley, R. E.; Wharton, L.; Levy, D. H. *J. Chem. Phys.* **1978**, *68*, 671.
(39) Smalley, R. F.; Wharton, L.; Levy, D. H. *J. Chem. Phys.* **1976**, *64*, 3266.
(40) Kowalski, K.; Piecuch, P. *J. Chem. Phys.* **2000**, *113*, 18. Kowalski, K.; Piecuch, P. *J. Chem. Phys.* **2005**, *122*, 074107.
(41) Bomble, Y. J.; Stanton, J. F.; Kállay, M.; Gauss, J. *J. Chem. Phys.* **2005**, *123*, 054101.
(42) Barletta, P.; Tennyson, J.; Barker, P. F. *Phys. Rev. A* **2008**, *78*, 052707.
(43) de Lara-Castells, M. P.; Prosmiti, R.; Delgado-Barrio, G.; López-Durán, D.; Villarreal, P.; Gianturco, F. A.; Jellinek, J. *Phys. Rev. A* **2006**, *74*, 054611.
(44) de Lara-Castells, M. P.; Prosmiti, R.; López-Durán, D.; Delgado-Barrio, G.; Villarreal, P.; Gianturco, F. A.; Jellinek, J. *Phys. Scr.* **2007**, *76*, C96.
(45) de Lara-Castells, M. P.; Prosmiti, R.; López-Durán, D.; Delgado-Barrio, G.; Villarreal, P.; Gianturco, F. A.; Jellinek, J. *Int. J. Quantum Chem.* **2007**, *107*, 2902.
(46) Boucher, D. S.; Darr, J. P.; Strasfeld, D. B.; Loomis, R. A. *J. Phys. Chem. A* **2008**, *112*, 13393.

JP901250U